

# CrystEngComm

rsc.li/crystengcomm



ISSN 1466-8033

**PAPER**











Edita Garskaite *et al.*

Assessing aspects of solution-based chemical synthesis  
to convert waste Si solar cells into nanostructured  
aluminosilicate crystals




Cite this: *CrystEngComm*, 2024, 26, 2233

# Assessing aspects of solution-based chemical synthesis to convert waste Si solar cells into nanostructured aluminosilicate crystals

Edita Garskaite, <sup>†\*ab</sup> Math Bollen, <sup>c</sup> Enock Mulenga, <sup>c</sup> Mathis Warlo, <sup>d</sup> Glenn Bark, <sup>d</sup> Espen Olsen, <sup>e</sup> Dalia Brazinskiene, <sup>f</sup> Denis Sokol, <sup>g</sup> Dietrich Buck <sup>a</sup> and Dick Sandberg <sup>a</sup>

The end-of-life recycling of crystalline silicon photovoltaic (PV) modules and the utilisation of waste is of fundamental importance to future circular-economy societies. In the present work, the wet-chemistry synthesis route – a low-temperature dissolution–precipitation process – was explored to produce aluminosilicate minerals from waste c-Si solar cells. Nanostructured crystals were produced in an alkaline medium by increasing the reaction temperature from room temperature to 75 °C. The morphology of the produced crystals varied from nanolayered aggregates to rod-shaped crystals and was found to be dependent on the temperature of the reaction medium. Chemical and phase composition studies revealed that the synthesised compounds consisted of structurally different phases of aluminosilicate minerals. The purity and elemental composition of produced crystals were evaluated by energy dispersive spectroscopy (EDS) and micro X-ray fluorescence (μXRF) analysis, confirming the presence of Al, O, and Si elements. These results give new insights into the processing of aluminosilicate minerals with sustainable attributes and provide a possible route to reducing waste and strengthening the circular economy.

Received 15th January 2024,  
Accepted 23rd March 2024

DOI: 10.1039/d4ce00038b

rsc.li/crystengcomm

## 1. Introduction

Solar power is an important renewable energy technology with the potential of significantly reducing greenhouse gas emission from electrical power production worldwide. In the last few decades, extensive development of photovoltaic (PV) technology reduced installation costs, and increasing policy support have resulted in numerous silicon (Si) based solar

panels being installed globally.<sup>1</sup> In the coming years, this is expected to increase.<sup>2</sup>

Crystalline silicon PV modules normally have a factory guaranteed lifespan of 25 years, with a minimum of 80% of original efficiency left. At the end of their design life, such devices are now considered electronic waste.<sup>3–6</sup> The EU Waste Electrical and Electronic Equipment (WEEE) regulations require manufacturers to collect and recycle used solar panels.<sup>4,5</sup> Yet, at the end of life, only some parts are recycled; the Si and laminates are either incinerated or sent to landfill.<sup>7–9</sup>

From the technological side, PV solar cells can be reused *via* processes relying primarily on physical treatments, such as crushing and milling. Some components can be thermally and chemically regained.<sup>1,4,9,10</sup> However, according to,<sup>4,10,11</sup> many aspects of solar cell waste processing need further improvement, as most of the implemented processes have drawbacks, like the substantial energy required to recover solar cell materials and/or negative consequences for the environment when considering the re-processing requirements. Finding economically viable methods with low environmental impact to recover or upcycle valuable solar-cell constituents reduces both the amount of waste and the amount of new material that needs to be mined. All this is of vital importance for strengthening the circular economy.

The published literature shows numerous studies dedicated to various synthesis methods and routes that aim to transform

<sup>a</sup> Wood Science and Engineering, Department of Engineering Sciences and Mathematics, Luleå University of Technology, Forskargatan 1, SE-931 87 Skellefteå, Sweden. E-mail: edita.garskaite@byggtek.lth.se

<sup>b</sup> Division of Building Materials, Lund University, John Ericssons väg 1, SE-221 00, Lund, Sweden

<sup>c</sup> Electric Power Engineering, Luleå University of Technology, Forskargatan 1, SE-931 87 Skellefteå, Sweden

<sup>d</sup> Geosciences and Environmental Engineering, Department of Civil, Environmental and Natural Resources Engineering, Luleå University of Technology, SE-971 87 Luleå, Sweden

<sup>e</sup> Department of Physics, Faculty of Science and Technology, Norwegian University of Life Sciences (NMBU), Drøbakveien 31, 1430 Ås, Norway

<sup>f</sup> Center for Physical Sciences and Technology, Sauletekio 3, LT-10257, Vilnius, Lithuania

<sup>g</sup> Institute of Chemistry, Faculty of Chemistry and Geosciences, Vilnius University, Naugarduko 24, Vilnius LT-03225, Lithuania

<sup>†</sup> The work was performed at Wood Science and Engineering, Department of Engineering Sciences and Mathematics, Luleå University of Technology, Forskargatan 1, SE-931 87 Skellefteå, Sweden.


waste PV materials into new materials. For example, Ding *et al.* have reported a solution-based synthesis method using sodium hydroxide (NaOH) to transform waste silicon sludge into silica (SiO<sub>2</sub>) nanoparticles of about 20–45 nm.<sup>12</sup> In another study, Bondareva *et al.* explored the hydrothermal synthesis route using different aqueous alkali solutions to convert bulk silicon into SiO<sub>2</sub> nanoparticles of 8–50 nm.<sup>13</sup> A wet-chemistry process for the simultaneous recovery of high-purity silver and silicon from waste solar cells combined with the reverse electroplating technique, which led to increased recovery yield of metals, has been also reported.<sup>14</sup> Recently, Sim *et al.* demonstrated the recovery of Si metal by using phosphoric acid (H<sub>3</sub>PO<sub>4</sub>) and upcycling it into materials for anodes in lithium-ion batteries.<sup>15</sup> In another study, the glass from a waste solar panel was treated by alkaline melting and hydrothermal synthesis with the aim of fabricating zeolite humidity control materials.<sup>16</sup> Attempts have also been made to recycle industrial by-products rich in silicon into materials that can be used as replacements for cement and concrete. For instance, an extensive review by Siddique and Chahal reports on the improvement of the quality of cement paste/mortar and concrete by using silica dust deposited from the fumes generated during Si production.<sup>17</sup> Fernandez *et al.* studied incorporation of solar PV cell waste in cement-based systems and its effect on the mechanical strength, porosity, and thermal insulation properties of the product.<sup>18</sup> A similar approach to use silica or re-utilise solar cell residue in construction materials has been also proposed by other research groups.<sup>19,20</sup> Evidently, efforts have been undertaken to produce new materials with specific structural features, *e.g.* crystal structure, crystallinity, micro-/nanostructure, particle size, and shape, as these are essential for the material to perform well in its intended applications.

With respect to aluminosilicates, these materials, due to the large variation in their structure and physicochemical properties,<sup>21</sup> are used extensively in everyday applications spanning from commercial adsorbents and catalysts<sup>22,23</sup> to the construction sector, *e.g.*, cement,<sup>24,25</sup> intumescent coatings,<sup>26–28</sup> and materials for stabilization of soft soil.<sup>29,30</sup> As previously noted, the material processing technique plays a vital role when aiming to convert a starting material into a useful form or a new material with controlled structural features and properties. In this context, solution-based chemical syntheses have several advantages, such as processing flexibility, environmental friendliness, and simplicity. Flexibility is related to the broad range of precursors, solvents, and organic additives, which can be selected to obtain materials with desirable structural and morphological features. From an environmental point of view, water is the preferred solvent. Another important factor for using such methods is the wide variety of solution parameters (concentration, pH, and temperature) and different processing conditions (temperature, reaction time, stirring rate, and pressure) that can be applied and varied. Thus, it is worthwhile to explore the processing of silicate-based minerals by wet-chemistry synthesis performed under mild conditions using an abundance of waste solar cells, and so allowing energy savings and reducing waste generation.

In the present work, rod-shaped aluminosilicate mineral-based crystals were synthesised by a low-temperature dissolution–precipitation process. A wet-chemistry synthesis route to convert used Si solar cells into aluminosilicates was assessed. The morphological features of the formed nanostructured crystals were evaluated using scanning electron microscopy (SEM), and the elemental composition and distribution were analysed with energy dispersive spectrometer (EDS) and micro X-ray fluorescence (μXRF). The phase composition and crystallinity of the product was studied by X-ray powder diffraction (XRD), and the chemical composition was evaluated by Fourier transform infrared (FTIR) spectroscopy. The morphological and structural properties of produced crystals were correlated to the synthesis conditions. The results obtained indicate the potential of the proposed process as an affordable, scalable, and easily adoptable material processing solution for converting waste Si solar cells into environmentally friendly minerals, and thereby contributing to the sustainable use of resources.

## 2. Experimental part

### 2.1. Processing of Si solar cells

Before processing, the as-received polycrystalline silicon (Si) solar cell materials were washed with ethanol (CH<sub>3</sub>CH<sub>2</sub>OH, 99.7%, European Pharmacopeia, SOLVECO, Rosersberg, Sweden) by sonicating for 5–10 min, then dried at room temperature. Dried pieces of solar cells were then ground in a planetary ball mill (Mono Mill Pulverisette 6, FRITSCH) for 30 min (200 rpm) to fine powders, herein designated as Si solar-cell powders. In the following step, 0.350 g of pulverised Si solar-cell powders were placed in a conical flask, and 30 mL of ammonia solution (NH<sub>4</sub>OH, 25%, Sigma-Aldrich, Lithuania) was added. The suspended powders were then stirred on a magnetic plate for 24 h. The conical flask was connected to a Vigreux distilling column to minimise the loss of ammonia. The pH of the initial reaction medium was measured to be 13.8, and the synthesis experiments were performed at room temperature (25 °C), 50 °C, and 75 °C. The pH of the reaction medium was measured 30 min, 1 h, and 24 h after the Si solar-cell powders were suspended in NH<sub>4</sub>OH. For these respective time points, the pH was 12.65, 12.13, and 12.30 for the reaction carried out at 25 °C; 11.00, 11.07, and 11.07 for the reaction at 50 °C; and 10.5, 10.5, and 9.75 for the reaction at 75 °C. The pH of the reaction medium was raised to ~13.00 by addition of NH<sub>4</sub>OH at 1 h and 24 h after the beginning of the reaction. Subsequently, 24 h after the synthesis, powders were decanted and washed with water and isopropanol.

### 2.2. Characterisation

The morphological features of the as-received Si solar cells before and after processing were evaluated using a field emission gun scanning electron microscope (FEG-SEM,



SU70, Hitachi) at the Institute of Chemistry infrastructure at Vilnius University. Secondary electron imaging was performed with an electron beam acceleration voltage of 2.0–5.0 kV. Before analysis, the powder samples were coated with a 10 nm layer of Ag. Elemental analysis was performed using a TM3000 Tabletop scanning electron microscope (SEM) (Hitachi), at the Institute of Chemistry infrastructure at Vilnius University, equipped with an energy dispersive X-ray spectrometer (EDS). The spectrometer was controlled by INCA software (Oxford Instruments). For morphological studies of the powders acquired after ball milling, backscattered electron images were recorded, with an electron beam acceleration voltage of 15 kV. An X-ray acquisition time of 315 s was used to obtain the EDS spectra (number of independent measurements ( $n$ ) = 3–5 for each feature of interest) and the elemental mapping images. In addition, powder materials of the synthesis experiment carried out at 75 °C was spread on a C-tape, attached to a metal stub sample holder, and mapped by SEM-EDS using a Zeiss Merlin field emission gun scanning electron microscope (FEG SEM) equipped with an Oxford Instruments 50 mm<sup>2</sup> X-Flash EDS detector and the Oxford Instruments AZtec software at the LUMIA (Luleå Material Imaging and Analysis) lab infrastructure at Luleå University of Technology. Mapping was performed at an electron beam acceleration voltage of 20 kV and a current of 1 nA using a cyclic scan that was run until significant changes were no longer observed on the chemical live images. Further, spot analyses on the same material by micro X-ray fluorescence ( $\mu$ XRF) using a Bruker M4 Tornado at Luleå University of Technology, equipped with a Rh X-ray tube and operated at 50 kV and 600  $\mu$ A, were carried out to confirm the composition of the material and detect potential impurities. The material phase composition was investigated by X-ray powder diffraction (XRD) analysis (MiniFlex II, Rigaku; Cu-K $\alpha$  radiation,  $\lambda$  = 0.1542 nm, 40 kV, 100 mA,  $2\theta$  = 5–70°) at the Institute of Chemistry infrastructure at Vilnius University. Infrared spectra were recorded using a Fourier transform infrared (FTIR) spectrometer (Frontier FT-IR, Perkin Elmer; ZnSe/Diamond ATR crystal, DTGS detector, 4000–600 cm<sup>−1</sup>, 4 scans) at the Wood Science and Engineering division infrastructure at the Luleå University of Technology.

### 3. Results and discussion

#### 3.1. Morphology evaluation

The SEM/EDS images of the top view of the untreated Si solar-cell sample, as presented in Fig. 1(a) and (b), show the typical morphology of the cell surface with a uniformly deposited Ag layer from a screen-printed contact finger. Examination of the samples showed distinct elemental compositions for different regions examined within a cell surface (Fig. 1(a)). The EDS spectra (Fig. 1(b)) and EDS-based elemental mapping (Fig. 1(b) (inset)) show that the studied surface contained the C, O, Al, Si and Ag elements. The Al element originated from the Ag front contact finger material or from the solder used to connect Ag fingers to busbar electrical leads. The Pb element was occasionally also detected and was principally distributed within the Ag plate; Pb originates from the cell metallisation pastes.<sup>31</sup> Furthermore, the SEM image of the ball-milled solar-cell pieces (Fig. 1(c)) shows that ground powders consist of larger particles with an average diameter of 0.5–1  $\mu$ m and smaller particles with sizes ranging to nanoscale.

SEM images of the powders from ball-milled solar-cell materials treated chemically at different temperatures (Fig. 2) show that after the treatment, a new material exhibiting layered growth morphology was formed. The material synthesised at room temperature (25 °C) consists of agglomerated structures homogeneously distributed on the entire surface of the initial undissolved grain (Fig. 2(a and b)). Images taken at higher magnification revealed that structures were formed of nanolayered crystals; the representative image is shown in Fig. 2(c). Crystals formed from the reaction mixtures heated to 50 °C (Fig. 2(d–f)) and 75 °C (Fig. 2(g–i)) possess obviously different morphologies. Examination of micromorphology showed that the synthesised crystals exhibit a hierarchical layered structure with elongated rod-shaped crystals. The length of these elongated homogeneous crystals ranges from about 1 to 2  $\mu$ m and the width ranges from about 100 to 200 nm (Fig. 2(f and i)). Comparing the crystals synthesised at 50 °C to those synthesised at 75 °C, a greater quantity of rod-shaped crystals, and with a longer average length, were obtained from the latter reaction mixture. This can be attributed to the direct effect of the temperature and the slight drop in pH, the details

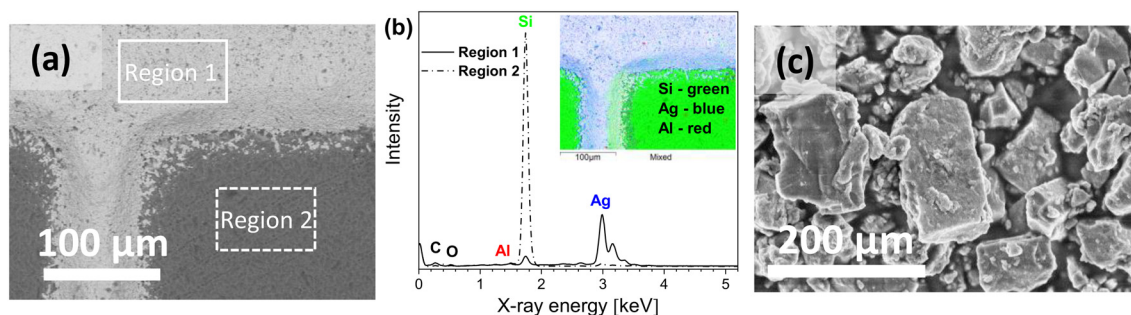


**Fig. 1** SEM/EDS images showing: (a) EDS region analysis of the surface of the Si solar-cell sample, (b) EDS spectra for studied regions marked in image (a) (inset: EDS mapping image of the same sample showing distribution of Al, Si and Ag), and (c) SEM image of the ball-milled Si solar cells.





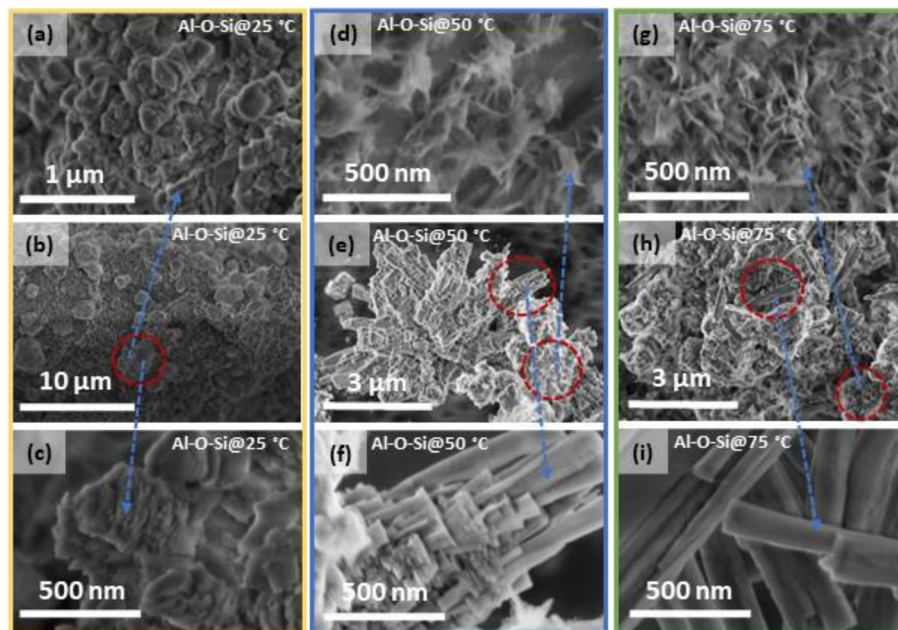


Fig. 2 SEM images showing morphological features of the (a–c) Si solar-cell powders treated at 25 °C (d–f) 50 °C, and (g–i) 75 °C. Red dashed circles in (b), (e), and (h) show the differently formed structures that are shown in the higher magnification images.

of which are presented in the experimental part of this study, as the dissolution and precipitation reactions are temperature- and pH-dependent. It was also observed that crystals grown from the reaction mixtures at elevated temperatures possess a more layered structure closer to the initial grain surface (Fig. 2(f)), compared to crystals grown at 25 °C; this is most likely due to the higher supersaturation. It is known that the energy barrier for nucleation is lower upon increasing the solution concentration. Therefore, crystals tend to nucleate more rapidly, which leads to the formation of many small crystals. The smoother morphology was observed on the surface of “elongated” crystals, indicating lower saturation of reactive species. Nucleation in diluted solutions has a slower growth, so larger crystals can be formed (Fig. 2(i)). SEM images further revealed that the surface of the powders, after the treatment at 50 °C and 75 °C, also possess places covered with spike-like structures (Fig. 2(d and g)), and these might be attributed to the presence of an additional silicate phase. Since the reaction product was studied after 24 h of synthesis, it is likely that surface passivation of the Si solar-cell grains occurred, and that the solubility limit of the host solid was reached under the current experimental conditions.

The SEM image in Fig. 3(a) shows a close-up of a sample chosen for further elemental mapping with EDS. The corresponding EDS spectra seen in Fig. 3(b) show the distribution of the observed elements in powders treated at 50 °C. The cyan line in the SEM image marks where the EDS line-based analysis was performed. The EDS analysis demonstrated that the rod-shaped crystals are composed of Si, Al, and O. Furthermore, the intensity of Al  $K\alpha$  and Si  $K\alpha$  peaks in the spectra vary along the entire analysed region, *i.e.*, the intensity of the Al  $K\alpha$  peak increased and the

intensity of the Si  $K\alpha$  peak decreased over segments of the regions covered by crystal structures, while the opposite tendency was observed over segments with fewer crystals or none (Fig. 3(b)). This is not surprising given the silicate matrix's ability to accommodate varying amounts of different ions as well as its great affinity to aluminium, which results in Al–O–Si networks.<sup>32,33</sup>

To aid in the identification of elements present within the synthesised crystals, an EDS-based mapping analysis was performed. SEM images with EDS-based elemental mapping of the representative rod-shaped crystals synthesised at 75 °C are shown in Fig. 3(c). Examining the X-ray maps of Si, Al, O, and C, distinct levels of intensity can be recognised, with aluminium exhibiting higher intensity throughout the synthesised crystals compared to that of silicon, clearly indicating the formation of an aluminosilicate-based phase within the reaction mixture.<sup>13,34</sup> Furthermore, morphology observations also confirmed that there was no surface textural variation among synthesised crystals that underwent the same treatment procedure, *e.g.* processed at 50 °C. The rod-shaped crystals appear finely distributed throughout the entire specimen with occasional formation of larger agglomerated clusters of newly synthesised mineral crystals (Fig. 3(a)). Nevertheless, this also suggests that processing conditions still need to be adjusted to achieve a higher degree of solar-cell material conversion.

With regard to the deposition of the aluminosilicate mineral in aqueous solution, several processes govern the dissolution and precipitation of the solid phase. The dissolution of Si solar-cell powders in  $\text{NH}_3$  aqueous solution leads to the formation of orthosilicic acid,  $\text{Si}(\text{OH})_4$ . When the concentration of  $\text{Si}(\text{OH})_4$  increases, it begins to polymerise



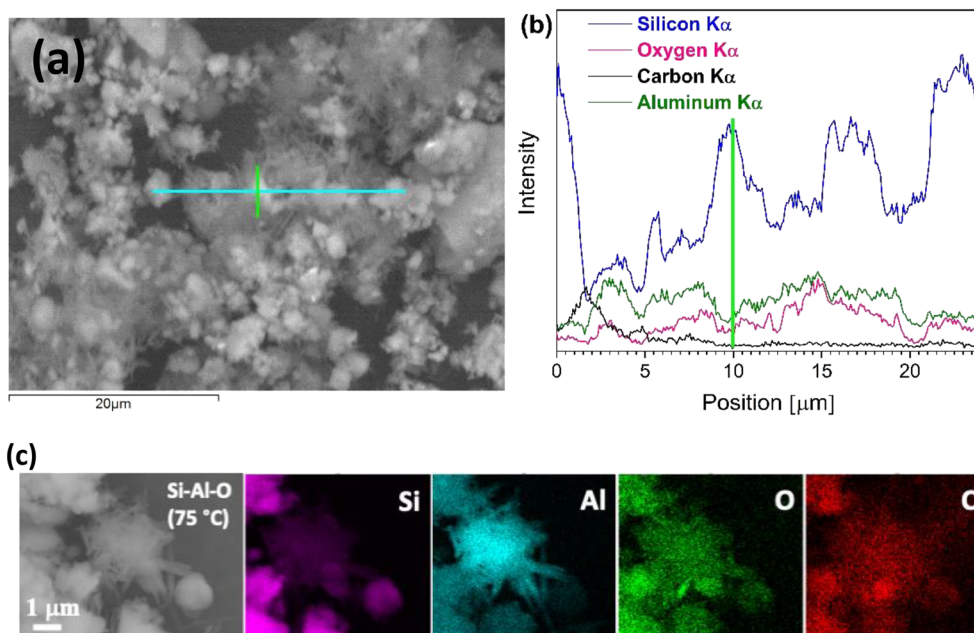


**Fig. 3** (a) SEM image of Si solar-cell powders processed at 50 °C and (b) corresponding EDS spectra showing the distribution of the Si, O, C, and Al elements within the studied region marked by the cyan line in (a). The green vertical line at 10  $\mu\text{m}$  in (b) corresponds to the position marked by the green line in (a). (c) SEM image and X-ray maps of processed Si solar-cells at 75 °C showing the distribution of Si, Al, O, and C elements within the studied area. Produced crystals show higher intensity for Al and lower intensity for Si, compared to less-reacted particles of solar cells.

and forms into amorphous silica gel.<sup>35</sup> At high pH and higher temperature, the solubility of amorphous silica increases, which suggests more species available to react in the solution. Aluminium ions in water are hydrated and, with increasing pH, exist as  $\text{Al}(\text{OH})_4^-$  species.<sup>36,37</sup> The pH of the present reaction medium was measured to be from 8 to 13. As previously mentioned, aluminium has a strong chemical affinity towards silicon, and this reduces the dissolution of silica. Thus, the formation of a solid phase containing Al–O–Si linkages is expected when the concentration gradient of reactive species is high. These processes are dependent upon pH, temperature, and concentration.

Interpretation of the growth mechanisms of crystals has been described elsewhere.<sup>38–42</sup> The formation of mineral crystals in the present reaction medium is governed by multiple mechanisms. Homogeneous or heterogeneous nucleation is followed by crystal growth. Earlier works reported that agglomeration of silicate particles in solution is concentration-dependent, and crystal growth can involve aggregation of initial amorphous particles followed by crystallisation.<sup>43</sup> Accordingly, the factors determining the size and shape of these crystals likely include the combined effects of bulk material dissolution and ionic species supply, their migration in solution as well as sorption during the oriented aggregation/attachment process. Although tuning of the morphology of the nanostructured crystals synthesised herein can be mainly ascribed to the reaction species, further investigations, *e.g.* transmission electron microscopy (TEM) studies, confirming the oriented aggregation of primary particles are still needed.<sup>42</sup>

Additionally, the  $\mu\text{XRF}$  analysis of powders processed at 75 °C was performed to confirm the elemental composition and check the presence of impurities (Fig. 4). Aside from the strong signals for Si and Al, several other elements, including Fe, Cu, Zn, Pb, and Bi, were detected; although control spots on nearly powderless parts of the sample holder suggest these elements come from the sample holder itself.

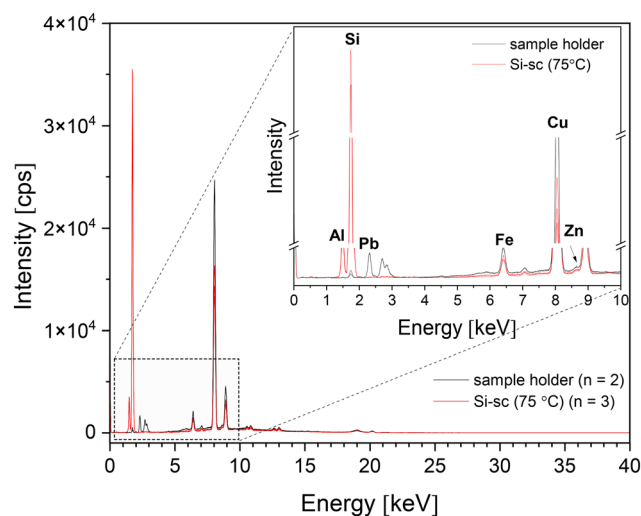


**Fig. 4**  $\mu\text{XRF}$  spectra showing the elemental composition of Si solar-cell powders processed at 75 °C (red,  $n = 3$ ) and of the sample holder without powder (black,  $n = 2$ ). Inset shows enlarged spectra region and lines assigned to particular elements. The lines of Al and Si are very distinct for the powder spectra but almost absent for spots in areas with next to no powder.



### 3.2. Structural studies

The XRD patterns of Si solar-cell powders before and after the chemical treatment were recorded to verify the phase composition of the synthesised material (Fig. 5). Sharply resolved Bragg reflections in the XRD pattern of untreated Si solar-cell powders were observed at  $2\theta = 29.12^\circ$ ,  $48.02^\circ$ ,  $56.78^\circ$  and  $69.82^\circ$ , and were assigned to the (111), (220), (131), and (040) diffraction peaks of the crystalline Si phase [JCPDS no. 96-152-6656]. The XRD patterns of Si solar-cell powders chemically treated at 25 °C, 50 °C, and 75 °C are distinct. In addition to the reflections assigned to the polycrystalline Si phase, reflections in the  $2\theta$  regions of 18–22° and 37–47° were observed, which were assigned to the silicate minerals containing Al–O–Si linkages. The indexing of the Al–Si mineral phase indicates that the dominant silicate phase mirrors the reflections of dialuminium silicate oxide ( $\text{Al}_2\text{O}_5\text{Si}$ ) [JCPDS no. 96-101-0330], although other aluminosilicate-based minerals are most likely also present. Furthermore, the XRD pattern of powders chemically treated at 50 °C showed a small reflection at  $2\theta = 8.7^\circ$ , which probably indicates the presence of phases containing a layered structure.<sup>44–47</sup> From the literature studies reported, it is apparent that the alumina–silica system is very complex,<sup>29,45,48,49</sup> and additional analyses, such as TEM and Rietveld refinement, will be required for a detailed identification of the crystal structure of the grown Al–O–Si phase. XRD results also showed that three different reaction systems (25 °C/50 °C/75 °C) gave different intensities and ratios of peaks at  $2\theta = 19.16^\circ$  and  $19.46^\circ$ , and at  $2\theta = 38.8^\circ$  and  $39.1^\circ$  (Fig. 5(insets)). This further suggests the formation of minerals with different crystalline phases. It also complements the SEM results and confirms that phase

composition and surface morphology of the coprecipitated minerals can be altered by changing the temperature in the reaction medium.

The produced samples were further examined by performing vibrational spectroscopy. FTIR spectra of the ball-milled solar-cell powders before and after treatment are shown in Fig. 6. The spectrum from the untreated powders showed no absorption bands attributed to Si–O/Al–O bonds, whilst spectra of the chemically treated powders exhibited different absorbances in the 1200–900  $\text{cm}^{-1}$  and 3700–3440  $\text{cm}^{-1}$  regions. The spectrum from the powders processed at 25 °C shows a broad absorption band in the 1100–900  $\text{cm}^{-1}$  region, which is composed of multiple overlapping bands with maxima located at 1054  $\text{cm}^{-1}$ , 964  $\text{cm}^{-1}$ , and 910  $\text{cm}^{-1}$ . These were assigned to Si–O stretching vibrations arising from silicate ( $\text{SiO}_4^{2-}$  group).<sup>50</sup> A small broad band located at 701  $\text{cm}^{-1}$  is attributed to the Al–O–Si bending vibrations in the tetrahedral framework.<sup>51</sup> The spectra recorded from the powders treated at 50 °C and 75 °C exhibited different spectral features in the 1200–900  $\text{cm}^{-1}$  region. The overlapping bands in this region usually contain a number of different vibration modes due to Si–O–Si stretch and Al–O–Si stretch. The notable differences in the band intensities and peak shapes as well as apparent positional shift of peak maxima might be assigned to the presence of structurally distinct phases of aluminosilicate minerals.<sup>44,52</sup> The observed shift of Si–O bands to higher frequencies, and the decrease in intensity of Si–O–Al bands suggest a continuous replacement of  $\text{Al}^{3+}$  for  $\text{Si}^{4+}$  in the framework, as has been previously reported.<sup>51</sup> In accordance with,<sup>53</sup> a shift to higher wavenumbers is associated with an increase in oxygen in the  $\text{SiO}_x$  system. Furthermore, processed powders exhibited broad absorption bands in the 3700–3440  $\text{cm}^{-1}$  region with maxima at 3661, 3553, and 3459  $\text{cm}^{-1}$ . These were most prominent for the powders processed at 75 °C. These bands

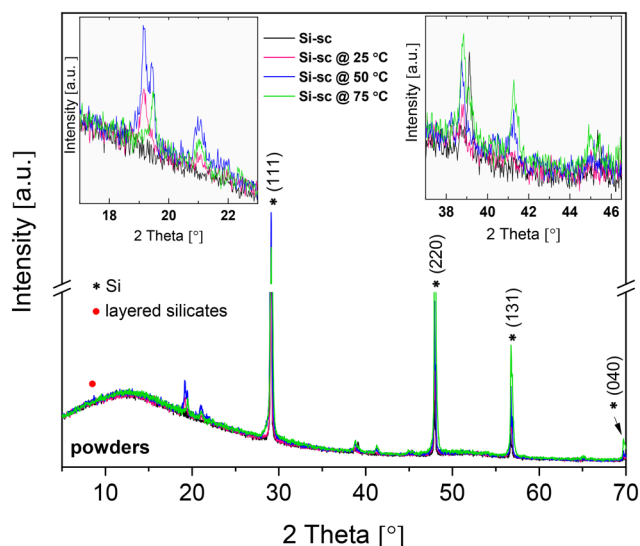


Fig. 5 XRD patterns of ball-milled Si solar cells (Si-sc) before and after the chemical treatment (insets: enlarged regions showing observed changes in the peak intensities). The red dot (•) marks the Bragg reflection at  $2\theta = 8.7^\circ$  indicating layered structure of the silicates.

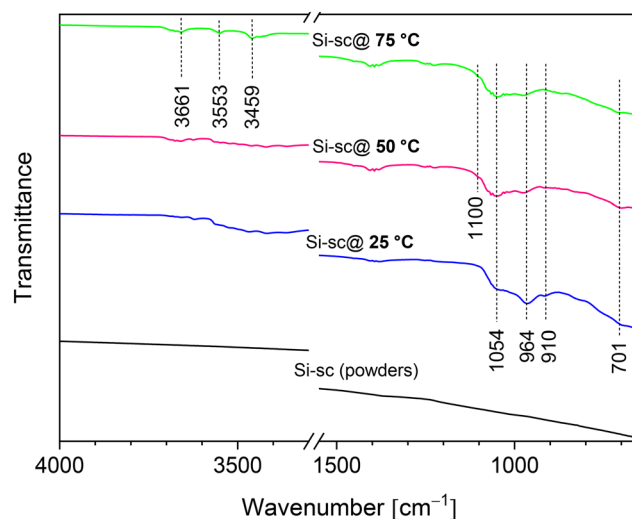


Fig. 6 FTIR spectra of ball-milled Si solar cells (Si-sc) before and after the chemical treatment.





could be ascribed to the Si–O(H)–Al and Al–OH groups,<sup>45,52</sup> which further confirms Al inclusion and formation of a Si–O–Al network.

Summarising the results obtained, it can be concluded that the relatively simple processing procedure herein proposed extends micro-structuring capabilities, which can lead to new physical properties and, subsequently, to new applications and functionality of aluminosilicate-based minerals. As noted above, the use of aluminosilicates in applications such as cement production is viable. However, a comprehensive approach from multiple areas of expertise will be required to ensure that important process components are attained, including proper material handling, quality control/quality assurance (QC/QA), performance characterization, and standardization. Ultimately, this could open the possibility to use up to ~1 billion tons of aluminosilicates in cement production globally. Thus, the results indicate a potential for this processing pathway in sustainable conversion of solar cells in decommissioned Si solar modules to products of value.

## 4. Conclusion

Aluminosilicate mineral crystals with variable morphological structure and phase composition have been synthesised from waste crystalline-Si solar cells through a low-temperature dissolution–precipitation process. The rod-shaped morphology and crystal length of nanostructured aluminosilicate mineral can be controlled by changing the temperature from 25 °C to 75 °C in the alkaline reaction medium. X-ray powder diffraction results showed that dialuminium silicate oxide (Al<sub>2</sub>O<sub>5</sub>Si) was the dominant crystalline phase and that different reaction systems (25 °C/50 °C/75 °C) gave different intensities and ratios of peaks at  $2\theta = 19.16^\circ$  and  $19.46^\circ$ , and at  $2\theta = 38.8^\circ$  and  $39.1^\circ$ , thus indicating that phase composition of the synthesised products can be favourably altered by changing the reaction temperature. Energy dispersive spectroscopy and micro X-ray fluorescence analyses confirmed the presence of the Al, O, and Si elements within formed crystals, verifying the formation of silicate minerals containing Al–O–Si linkages. Along with the proposed affordable, scalable, and easily adoptable processing route, the findings suggest a pathway of converting waste Si solar-cells into materials of value, reducing waste, and contributing to sustainability in the solar-energy value chain.

## Author contributions

Edita Garskaite – conceptualization, methodology, investigation, visualization, writing – original draft, and funding acquisition; Math Bollen – conceptualization, project administration, and writing – review and editing; Enock Mulenga – methodology; Mathis Warlo – investigation and data curation; Glenn Bark – investigation and data curation; Espen Olsen – resources, and writing – review and editing; Dalia Brazinskiene – resources and contributed to data analysis; Denis Sokol – methodology and investigation; Dietrich Buck – visualization, writing – review and

editing, and contributed to data analysis; Dick Sandberg – funding acquisition and writing – review and editing. All authors discussed the results and commented on the manuscript.

## Conflicts of interest

The authors declare that they have no known competing financial interests or personal relationships that could appear to influence the work reported in this paper.

## Acknowledgements

This project was funded by the Rönnbäret Foundation, Skellefteå Municipality, Sweden (2022–2023). Edit Garskaite thanks Prof. Paul Sandberg “CemVision AB”/Lund University for valuable discussions regarding cement production. Prof. Espen Olsen (NMBU, Norway) provided solar-cell samples.

## References

- 1 F. C. S. M. Padoan, P. Altimari and F. Pagnanelli, *Sol. Energy*, 2019, **177**, 746–761.
- 2 International Energy Agency (IEA), Renewable Energy Market Update, Outlook for 2023 and 2024, 2023, p. 89, [https://www.oecd-ilibrary.org/energy/renewable-energy-market-update\\_89017c62-en](https://www.oecd-ilibrary.org/energy/renewable-energy-market-update_89017c62-en).
- 3 M. S. Chowdhury, K. S. Rahman, T. Chowdhury, N. Nuthammachot, K. Techato, M. Aktaruzzaman, S. K. Tiong, K. Sopian and N. Amin, *Energy Strat. Rev.*, 2020, **27**, 100431.
- 4 G. A. Heath, T. J. Silverman, M. Kempe, M. Deceglie, D. Ravikumar, T. Remo, H. Cui, P. Sinha, C. Libby, S. Shaw, K. Komoto, K. Wambach, E. Butler, T. Barnes and A. Wade, *Nat. Energy*, 2020, **5**(7), 502–510.
- 5 J.-K. Choi and V. Fthenakis, *J. Cleaner Prod.*, 2014, **66**, 443–449.
- 6 S. Ovaitt, H. Mirlet, S. Seetharaman and T. Barnes, *iScience*, 2022, **25**(1), 103488.
- 7 S. Mahmoudi, N. Huda, Z. Alavi, M. T. Islam and M. Behnia, *Resour., Conserv. Recycl.*, 2019, **146**, 1–16.
- 8 F. Cucchiella, I. D'Adamo and P. Rosa, *Renewable Sustainable Energy Rev.*, 2015, **47**, 552–561.
- 9 X. Wang, X. Tian, X. Chen, L. Ren and C. Geng, *Sol. Energy Mater. Sol. Cells*, 2022, **248**, 111976.
- 10 C. C. Farrell, A. I. Osman, R. Doherty, M. Saad, X. Zhang, A. Murphy, J. Harrison, A. S. M. Vennard, V. Kumaravel, A. H. Al-Muhtaseb and D. W. Rooney, *Renewable Sustainable Energy Rev.*, 2020, **128**, 109911.
- 11 D. Lin, Z. Liu, X. Li, Z. Cao and R. Xiong, *Clean Energy*, 2023, **7**(3), 532–546.
- 12 H. Ding, J. Li, Y. Gao, D. Zhao, D. Shi, G. Mao, S. Liu and X. Tan, *Powder Technol.*, 2015, **284**, 231–236.
- 13 J. V. Bondareva, T. F. Aslyamov, A. G. Kvashnin, P. V. Dyakonov, Y. O. Kuzminova, Y. A. Mankelevich, E. N. Voronina, S. A. Dagesyan, A. V. Egorov, R. A. Khmel'nitsky, M. A. Tarkhov, N. V. Suetin, I. S. Akhatov and S. A. Evlashin, *ACS Sustainable Chem. Eng.*, 2020, **8**(37), 14006–14012.





- 14 R. Deng, P. R. Dias, M. M. Lunardi and J. Ji, *Green Chem.*, 2021, **23**(24), 10157–10167.
- 15 Y. Sim, Y. B. Tay, X. Lin Ankit and N. Mathews, *Sol. Energy Mater. Sol. Cells*, 2023, **257**, 112394.
- 16 Y.-W. Lin, W.-H. Lee and K.-L. Lin, *J. Mater. Res. Technol.*, 2022, **19**, 4128–4140.
- 17 R. Siddique and N. Chahal, *Resour., Conserv. Recycl.*, 2011, **55**(8), 739–744.
- 18 L. J. Fernández, R. Ferrer, D. F. Aponte and P. Fernandez, *Sol. Energy Mater. Sol. Cells*, 2011, **95**(7), 1701–1706.
- 19 B. Lothenbach, K. Scrivener and R. D. Hooton, *Cem. Concr. Res.*, 2011, **41**(12), 1244–1256.
- 20 G. Quercia, J. J. G. van der Putten, G. Husken and H. J. H. Brouwers, *Cem. Concr. Res.*, 2013, **54**, 161–179.
- 21 W. J. Mortier, *J. Catal.*, 1978, **55**(2), 138–145.
- 22 J. M. P. F. Silva, E. B. Silveira, A. L. H. Costa, C. O. Veloso, C. A. Henriques, F. M. Z. Zotin, M. L. L. Paredes, R. A. Reis and S. S. X. Chiaro, *Ind. Eng. Chem. Res.*, 2014, **53**(41), 16000–16014.
- 23 C. Belver, P. Aranda and E. Ruiz-Hitzky, *J. Mater. Chem. A*, 2013, **1**(25), 7477–7487.
- 24 F. Pacheco-Torgal, Z. Abdollahnejad, S. Miraldo, S. Baklouti and Y. Ding, *Constr. Build. Mater.*, 2012, **36**, 1053–1058.
- 25 J. L. Provis and S. A. Bernal, *Annu. Rev. Mater. Res.*, 2014, **44**, 299–327.
- 26 P. V. Krivenko, S. G. Guzii, L. Bodnarova, J. Valek, R. Hela and J. Zach, *J. Build. Eng.*, 2016, **8**, 14–19.
- 27 M.-B. Watolla, G. J. G. Gluth, P. Sturm, W. D. A. Rickard, S. Kruger and B. Schartel, *J. Ceram. Sci. Technol.*, 2017, **8**, 351–364.
- 28 B. Ulusoy, A. Fu, H. Ahmadi, K. Dam-Johansen and H. Wu, *J. Coat. Technol. Res.*, 2023, **20**(1), 233–248.
- 29 F. Ayub and S. A. Khan, *Constr. Build. Mater.*, 2023, **404**, 133195.
- 30 P. Sargent, The development of alkali-activated mixtures for soil stabilisation, in *Handbook of Alkali-Activated Cements, Mortars and Concretes*, ed. F. Pacheco-Torgal, J. A. Labrincha, C. Leonelli, A. Palomo and P. Chindaprasirt, Woodhead Publishing (Elsevier), 2015, ch. 21, pp. 555–604.
- 31 B. Jung, J. Park, D. Seo and N. Park, *ACS Sustainable Chem. Eng.*, 2016, **4**(8), 4079–4083.
- 32 S. Aramaki and R. Roy, *J. Am. Ceram. Soc.*, 1962, **45**(5), 229–242.
- 33 I. Garcia-Lodeiro, A. Palomo, A. Fernandez-Jimenez and D. E. Macphree, *Cem. Concr. Res.*, 2011, **41**(9), 923–931.
- 34 R. Dupuis, S. H. Hahn, A. C. T. van Duin, R. J. M. Pellenq and A. Poulesquen, *Phys. Chem. Chem. Phys.*, 2022, **24**(16), 9229–9235.
- 35 G. A. Blomfield and L. H. Little, *Can. J. Chem.*, 1973, **51**(11), 1771–1781.
- 36 J. Gregory and J. Duan, *Pure Appl. Chem.*, 2001, **73**(12), 2017–2026.
- 37 T. W. Swaddle, J. Salerno and P. A. Tregloan, *Chem. Soc. Rev.*, 1994, **23**(5), 319–325.
- 38 B. Fritz and C. Noguera, *Rev. Mineral. Geochem.*, 2009, **70**(1), 371–410.
- 39 T. W. Swaddle, *Coord. Chem. Rev.*, 2001, **219–221**, 665–686.
- 40 B. B. V. Salzmann, M. M. van der Sluijs, G. Soligno and D. Vanmaekelbergh, *Acc. Chem. Res.*, 2021, **54**(4), 787–797.
- 41 X. Xue, R. L. Penn, E. R. Leite, F. Huang and Z. Lin, *CrystEngComm*, 2014, **16**(8), 1419–1429.
- 42 R. L. Penn and J. A. Soltis, *CrystEngComm*, 2014, **16**(8), 1409–1418.
- 43 M. Kley, A. Kempter, V. Boyko and K. Huber, *Langmuir*, 2017, **33**(24), 6071–6083.
- 44 D. Tan, P. Yuan, F. Annabi-Bergaya, D. Liu and H. He, *Sci. Rep.*, 2015, **5**(1), 8870.
- 45 S. Li, H. He, Q. Tao, P. Du, A. Chen, Y. He and J. Zhu, *ACS Earth Space Chem.*, 2022, **6**(7), 1930–1936.
- 46 A. Bolshakov, M. van Diepen, A. J. F. van Hoof, D. E. Romero Hidalgo, N. Kosinov and E. J. M. Hensen, *ACS Appl. Mater. Interfaces*, 2019, **11**(43), 40151–40162.
- 47 S. Gaber, D. Gaber, I. Ismail, S. Alhassan and M. Khaleel, *CrystEngComm*, 2019, **21**(11), 1685–1690.
- 48 F. Pienkoß, C. Ochoa-Hernandez, N. Theyssen and W. Leitner, *ACS Sustainable Chem. Eng.*, 2018, **6**(7), 8782–8789.
- 49 J. Klinowski and T. L. Barr, *Acc. Chem. Res.*, 1999, **32**(8), 633–640.
- 50 E. San Andrés, A. del Prado, F. L. Martinez, I. Martil, D. Bravo and F. J. Lopez, *J. Appl. Phys.*, 2000, **87**(3), 1187–1192.
- 51 S. Jakobsson, *Appl. Spectrosc.*, 2002, **56**(6), 797–799.
- 52 A. A. Gabrienko, I. G. Danilova, S. S. Arzumanov, L. V. Pirutko, D. Freude and A. G. Stepanov, *J. Phys. Chem. C*, 2018, **122**(44), 25386–25395.
- 53 J. Holm and J. T. Roberts, *Langmuir*, 2007, **23**(22), 11217–11224.

